ACTA IMEKO
ISSN: 2221-870X
December 2026, Volume 15, Number 4, 1 – 8

Stress-wave propagation across material interfaces in multimaterial metallic specimens produced by laser powder bed fusion

Petr Zlámal[1], Jan Falta[1], Radim Dvořák[1]

[1] *Czech Technical University in Prague, Faculty of Transportation Sciences, Prague, Czechia*

ABSTRACT
The propagation of short broadband stress waves across a material interface in additively manufactured multimaterial specimens was experimentally investigated. Cylindrical CuCr1Zr–13Ni400 specimens produced by laser powder bed fusion were tested using a Forward Direct Impact Hopkinson Bar with a striker length of 5 mm. Strain gauges were positioned immediately before and after the internal material interface, allowing the wave response to be examined locally in both propagation directions. Geometrically identical single-material specimens were used as references. The experiments were performed in the elastic regime, enabling repeated impacts on the same specimens. The material interface produced measurable changes in the temporal shape of the stress pulse, with deviations from the homogeneous reference occurring at times consistent with the expected arrival of reflected wave components. The response depended on the direction of wave propagation across the interface. The FFT analysis also revealed changes in the relative frequency content, particularly at the measurement position before the interface. Similar reductions in stress and spectral amplitude were observed during propagation in both homogeneous and multimaterial specimens, demonstrating the significant influence of propagation and dispersion in the finite cylindrical geometry. The results show that the measured response results from the combined effects of interface interaction, broadband excitation, and dispersive wave propagation.

Section: RESEARCH PAPER

Keywords: Hopkinson bar; metallic multimaterial; stress-wave propagation; strain gauge

Citation: P. Zlámal, J. Falta, R. Dvořák, Stress-wave propagation across material interfaces in multimaterial metallic specimens produced by laser powder bed fusion, Acta IMEKO, vol. 15 (2026) no. 4, pp. 1–8. DOI: 10.21014/actaimeko.v15i4.2512

Section Editor: Daniel Kytyr, Czech Academy of Sciences, Czechia

Received: September 18, 2026; **In Final Form:** November 6, 2026; **Published:** December 2026.

Copyright: This is an open-access article distributed under the terms of the Creative Commons Attribution 4.0 International License.

Funding: The research was supported by the Czech Science Foundation in project no. 24-11505S.

Corresponding Author: Petr Zlámal, e-mail: zlamal@fd.cvut.cz

1. INTRODUCTION

The increasing ability to combine dissimilar metallic materials within a single additively manufactured component creates new opportunities for structures with spatially tailored properties. Multimaterial additive manufacturing makes it possible to introduce deliberate changes in mechanical, thermal, or other functional characteristics within one part [1]. Such material combinations have also been demonstrated in metal components produced by laser powder bed fusion (LPBF) [2]. However, from the point of view of dynamic loading, an interface between materials is not merely a geometrical feature: it constitutes a discontinuity encountered by a propagating stress wave.

For an ideal one-dimensional elastic wave, interaction with a perfectly bonded interface between two materials can be described in terms of their mechanical impedances: part of the incident wave is transmitted and part is reflected. In a finite real specimen, the measured response is also affected by the geometry of the sample, the character of the interface region, the duration and frequency content of the excitation, and the distance between the interface and the measurement location. Measurements performed directly on both sides of a material interface can, therefore, provide a more local view of the waveform evolution than measurements obtained only after propagation through the complete specimen.

Hopkinson-bar techniques provide a suitable platform for generating and recording short-duration stress waves. Although conventionally used for high-strain-rate material characterisation, Hopkinson-bar systems are also used as mechanical shock-excitation devices in dynamic metrology, where the spectral content of the excitation and the amplitude and phase response of the measurement chain are important for interpretation of the recorded signal [3], [4]. The measured signals can therefore also be analysed in the frequency domain. In our previous work, a Hopkinson-bar arrangement was adapted specifically for broadband elastic-wave measurements using millimetre-scale projectiles

[5]. The shortening of the projectile increased the high-frequency content of the generated pulse, but the upper-frequency part of the response was progressively modified with increasing propagation distance. A striker length of 5 mm provided a useful compromise between broadband excitation and experimental repeatability, while the experiments also demonstrated the importance of locating the measurement point close to the region of interest [5].

The present study extends this concept to an LPBF-manufactured multimaterial specimen. Strain gauges are positioned directly on opposite sides of the internal material interface, allowing the wave to be recorded shortly before and after it crosses the material interface. A striker length of 5 mm is used to generate a short broadband pulse, and the measured strain histories are analysed in both the time and frequency domains using the Fast Fourier Transform (FFT).

Interpretation of these measurements requires consideration of dispersion. The one-dimensional bar theory assumes wavelengths sufficiently large compared with transverse dimensions, for which the longitudinal wave velocity approaches $c_0 = \sqrt{E/\rho}$. At higher frequencies, radial inertia becomes important and longitudinal wave propagation in a cylindrical rod is described more accurately by the Pochhammer–Chree solution. The resulting frequency dependence of the phase velocity was demonstrated by Bancroft [6] and has been extensively investigated in Hopkinson-bar measurements [7], [8]. Consequently, broadband pulses undergo dispersive changes in shape and amplitude during propagation, even in homogeneous specimens. At sufficiently high frequencies, additional longitudinal modes may also contribute to the measured response [9]. Therefore, waveform differences between measuring positions cannot be attributed exclusively to the material interface.

The FFT analysis used here is therefore intended to characterise the experimentally observed spectral content before and after the material interface, rather than to determine a direct frequency-dependent transmission coefficient of the interface. The recorded signals contain the combined effects of interaction with the interface, propagation through the constituent materials, cylindrical-wave dispersion, and finite specimen geometry.

The objective of this study is to experimentally investigate the propagation of short broadband stress waves through LPBF-manufactured CuCr1Zr-13Ni400 multimaterial specimens. Cylindrical specimens containing a single material interface normal to the propagation direction are subjected to direct impact by a 5 mm long striker. The strain is measured immediately before and after the interface and subsequently on the transmission bar, and both orientations of the material interface are investigated. The study focuses on the directly measured time histories and their frequency spectra. No dispersion correction is applied to reconstruct an idealised one-dimensional waveform at the interface; instead, the known dispersive character of the broadband pulse is considered when interpreting the measured differences.

2. MATERIALS AND METHODS

2.1. Specimens and instrumentation

The samples were manufactured at Brno University of Technology using the LPBF technique, where the combination of CuCr1Zr and maraging steel 13Ni400 material has previously been investigated in the multimaterial processing of LPBF [10]. The experimental campaign included both multimaterial specimens and single-material reference specimens.

The material properties were determined from separate tensile specimens manufactured from the same metal powders using identical LPBF process parameters and heat treatment as the specimens investigated in this study. The experimentally determined properties are summarised in Table 1.

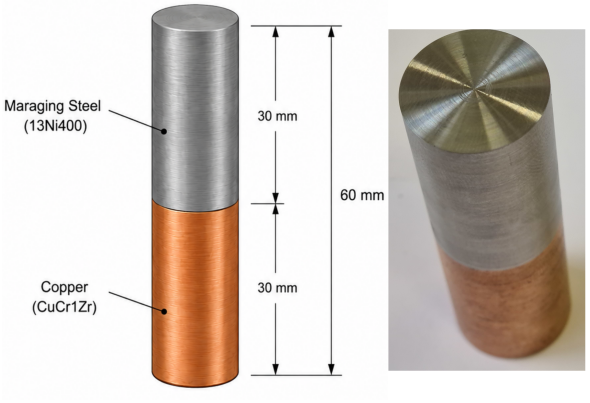


Figure 1. LPBF-manufactured CuCr1Zr–13Ni400 specimen: specimen geometry (left); manufactured sample (right).

Table 1. Experimentally determined material properties of the LPBF-manufactured CuCr1Zr and 13Ni400 alloys.

Property	CuCr1Zr	13Ni400
Young's modulus in GPa	93.6 ± 11.3	213.0 ± 12.3
Yield strength in MPa	374.6 ± 12.3	–
Density in kg/m^3	8164.2 ± 11.8	8814.1 ± 25.8

The yield strength of heat-treated 13Ni400 could not be reliably determined from the tensile tests due to its high hardness and limited ductility. However, a higher yield strength is expected compared with the corresponding as-built material, for which a value of (1102.5 ± 217.1) MPa was measured.

All specimens had a cylindrical geometry with a nominal diameter of 20 mm and a total length of 60 mm. The multimaterial specimens consisted of two 30 mm long sections of CuCr1Zr and 13Ni400, resulting in a planar material interface at the specimen mid-plane. The interface was oriented normal to the specimen axis and, therefore, perpendicular to the nominal direction of stress-wave propagation. The single-material reference specimens had the same external geometry, allowing the response of the multimaterial specimens to be compared with wave propagation through geometrically identical homogeneous specimens. The geometry of the specimen and the manufactured sample are shown in Figure 1. Two multimaterial specimens were manufactured, together with one single-material reference specimen of each constituent material, giving a total of four specimens. The selected impact conditions produced stresses within the elastic range of the specimen materials, so no permanent deformation of the specimens was expected. Consequently, repeated impacts could be performed on the same specimen, allowing several valid measurements to be obtained without the need for a separate specimen for each test. This repeatability of the elastic loading regime allowed the experimental campaign to be carried out using a relatively small number of specimens.

Each specimen was instrumented directly with four foil strain gauges (1-LY11-0.6/120, HBM, Germany). The gauges had a measuring-grid length of 0.6 mm, a nominal resistance of 120 Ω, and a gauge factor of approximately 1.8. Two measuring cross-sections, denoted MP1 and MP2, were located at axial positions of 15 mm and 45 mm from the impacted face, respectively. For the multimaterial specimens, these positions corresponded to distances of 15 mm before and 15 mm after the material interface.

At each measuring cross-section, two strain gauges were bonded to the specimen surface at diametrically opposite locations,

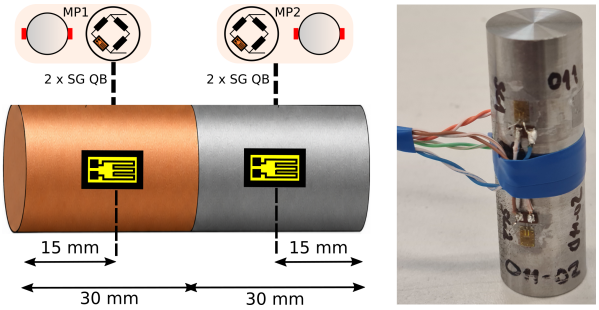


Figure 2. Instrumentation of the specimen: schematic of the specimen instrumentation (left); instrumented 13Ni400 reference specimen (right).

Striker	Specimen	Trans. bar
316L	13Ni400	316L
CuCr1Zr	CuCr1Zr	CuCr1Zr
316L	13Ni400	CuCr1Zr	CuCr1Zr
CuCr1Zr	CuCr1Zr	13Ni400	316L

Figure 3. Overview of the tested striker–specimen–transmission-bar material configurations, including the single-material reference tests and both orientations of the CuCr1Zr–13Ni400 multimaterial specimen.

180 ° apart in the circumferential direction, and aligned with the specimen axis to measure the axial strain. Each gauge was connected in a quarter-bridge configuration. The use of two opposing gauges at each MP enabled the uniformity of axial loading to be assessed and possible bending caused by imperfect alignment or a non-planar impact to be identified. Obtaining nearly identical signals from both strain gauges at the MP closest to the impact zone was crucial for assessing the validity of the test. The same instrumentation arrangement was used for both the single-material and multimaterial specimens, providing directly comparable strain measurements at identical axial positions. A schematic of the instrumentation and a photograph of the instrumented 13Ni400 reference specimen are shown in Figure 2.

2.2. Experimental setup

The experiments were performed using an in-house Hopkinson-bar apparatus configured as a Forward Direct Impact Hopkinson Bar. In this configuration, the specimen was placed in direct contact with the transmission bar and impacted directly by a short cylindrical striker. Throughout the experimental campaign, a striker length of 5 mm was used to generate a short, broadband stress pulse while maintaining sufficient repeatability of the impact, as established in the preceding calibration study [5].

Due to its short length, the striker was mounted on the front face of a hollow cylindrical carrier manufactured from PLA using 3D printing. The carrier ensured stable guidance of the striker inside the gas-gun barrel, preventing tilting or jamming during acceleration. Its wall thickness was approximately 0.4 mm, corresponding to the minimum thickness achievable with the printing process and selected to minimise the axial stiffness of the carrier relative to the metallic striker. The carrier was not separated from the striker prior to impact but acted as a sacrificial component, impacting together with the striker. The striker–carrier arrangement is described in more detail in [5].

Two transmission bars were used depending on which material formed the end of the specimen adjacent to the transmission bar. A CuCr1Zr transmission bar was used when the stress wave exited the specimen through CuCr1Zr. For configurations in which 13Ni400 maraging steel was in contact with the transmission bar, a bar made of EN 1.4404 (AISI 316L) stainless steel was used, since a 13Ni400 bar with the required dimensions was not available. Based on the experimentally determined properties of 13Ni400 and tabulated properties of EN 1.4404 ($E = 200$ GPa and $\rho = 8000$ kg/m^3), the estimated one-dimensional stress reflection coefficient at the specimen–bar interface is approximately -4.0 %. The corresponding reflected-wave amplitude is therefore relatively small compared with the incident wave. Moreover, the primary analysis presented in this study is focused on the strain signals recorded directly on the specimen before and after the CuCr1Zr–13Ni400 material interface; the signals measured on the transmission bar are used only to characterise the subsequent propagation of the stress wave.

The four material configurations used in the experimental campaign, including the two single-material reference tests and the two orientations of the multimaterial specimen, are summarised in Figure 3.

The transmitted wave was additionally recorded at two positions on the transmission bar. MP3 was located 15 mm from the specimen–bar interface and instrumented with two strain gauges positioned 180 ° apart around the circumference, while MP4 was located 296 mm from the interface and instrumented with a single gauge. All transmission-bar gauges were of type 1-LY61-1.5/120 (HBM, Germany), with a 1.5 mm measuring grid, a nominal resistance of 120 Ω, and a gauge factor of approximately 1.9. They were connected in quarter-bridge configurations. A schematic of the experimental setup and a photograph of the corresponding experimental arrangement are shown in Figure 4.

The strain gauge signals were amplified using low-noise differential amplifiers (EL-LNA-2, Elsys AG, Switzerland) with a gain of 100, and recorded simultaneously using a TraNET EPC high-speed data-acquisition system (Elsys AG, Switzerland). The sampling frequency was 10 MHz per channel, providing sufficient temporal resolution for the short-duration stress pulses and their subsequent frequency-domain analysis.

The striker was accelerated pneumatically, and the nominal impact velocity was approximately 10.5 m/s. The selected impact conditions kept the specimen response within the elastic range, allowing repeated impacts on the same instrumented specimen. Before each test, particular attention was paid to the coaxial alignment of the striker, specimen, and transmission bar, and to the parallelism of their contact surfaces.

2.3. Signal processing and frequency-domain analysis

For MP1 and MP2 on the specimen, the signals from the two strain gauges positioned 180 ° apart around the circumference were averaged to obtain a representative axial strain history. The averaged strain signals were subsequently converted into stress histories using the elastic modulus of the corresponding material at the given measuring position. This conversion was particularly important for MP2, where the material at the measuring location differs between the single-material reference and the multimaterial specimen. Direct comparison of strain histories would therefore not provide an equivalent representation of the propagating stress wave due to the different elastic moduli of CuCr1Zr and 13Ni400. The resulting averaged stress histories were used for subsequent time- and frequency-domain analyses. The FFT was calculated from the averaged time-domain waveforms rather than from individual impact records. Consequently, the frequency-domain res-

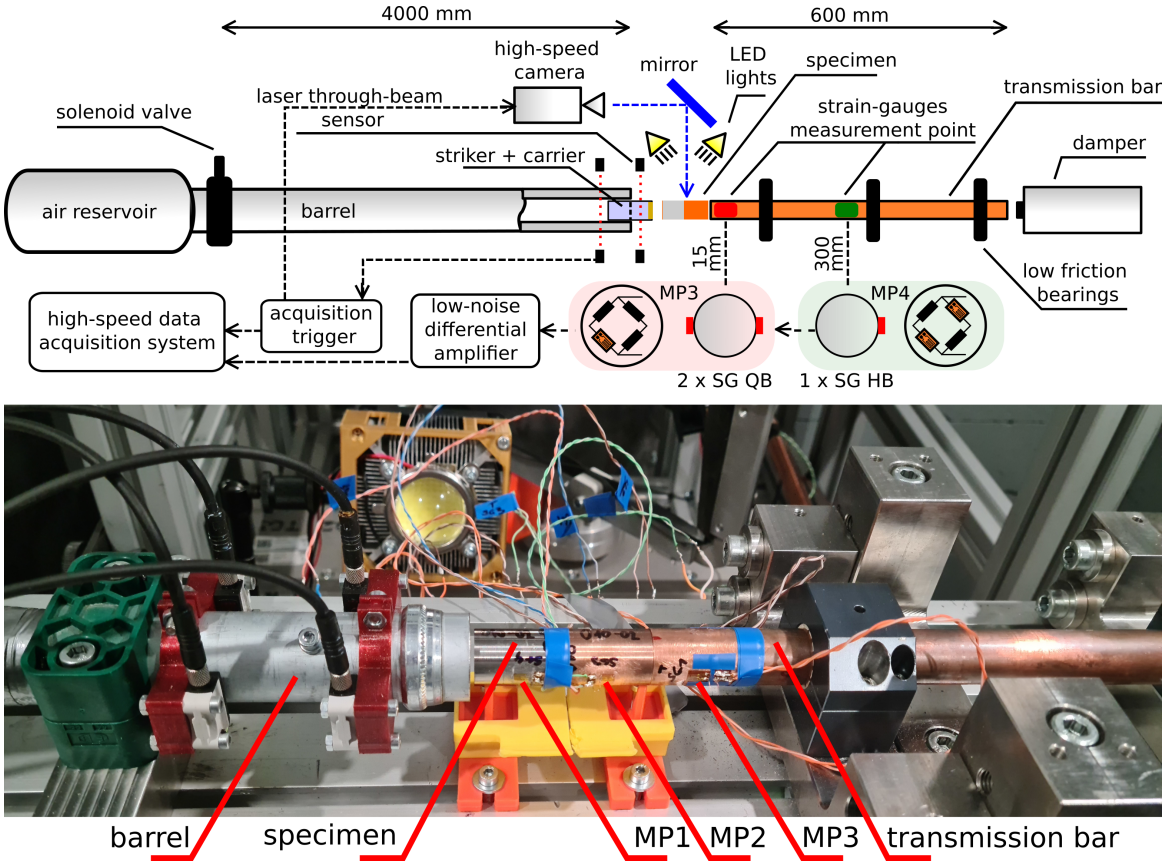


Figure 4. Experimental setup: scheme depicting the main components (top); corresponding experimental arrangement used during testing (bottom).

ults represent the spectral content of the mean response, without explicitly showing the variability between repeated impacts.

The frequency content of the measured stress pulse was evaluated using the FFT. For each measuring position, a time interval containing the first stress pulse was extracted from the signal recorded at a sampling frequency of 10 MHz. The same time-window duration was used for MP1 and MP2 to obtain identical frequency resolution and enable direct comparison of the resulting spectra. Prior to the FFT, the signal offset was removed using the unloaded part of the record.

The single-sided amplitude spectra obtained at MP1 and MP2 were compared to evaluate the evolution of the frequency content between the measuring positions before and after the material interface. For each signal, the single-sided amplitude spectrum was calculated from the FFT of the windowed time-domain signal. A Tukey window with a tapering parameter of $\alpha = 0.1$ was applied to reduce spectral leakage while only mildly attenuating the signal near the boundaries of the analysed time interval. The spectral amplitudes were corrected for the coherent gain of the applied window according to

$$A(f) = \frac{2\,|X(f)|}{\sum_{n=0}^{N-1} w(n)}, \tag{1}$$

where $X(f)$ is the discrete Fourier transform of the windowed signal, $w(n)$ is the applied window function, and N is the number of samples. The factor of two accounts for the use of the single-sided spectrum, except for the DC component and, for even N, the Nyquist component.

In addition to the absolute spectra, normalised amplitude spectra were calculated to compare the relative distribution of the frequency content independently of the absolute stress amplitude. The normalised spectrum was defined as

$$A_{\mathrm{norm}}(f) = \frac{A(f)}{A_{\max}}, \tag{2}$$

where $A_{\max}$ is the maximum amplitude of the corresponding spectrum. Thus, the maximum amplitude of each spectrum is equal to unity.

The comparison of MP1 and MP2 spectra was used to characterise changes in the amplitude and frequency distribution of the measured stress pulse between the two measuring positions. For the multimaterial specimens, MP1 and MP2 were located in different materials with different mechanical impedances and wave velocities. Consequently, the observed spectral differences reflect the combined effects of wave reflection and transmission at the material interface, propagation through the constituent materials, dispersion, and finite specimen geometry.

The comparison was therefore not interpreted as a direct frequency-dependent transmission coefficient or as a quantitative measure of energy attenuation. Instead, the absolute and normalised spectra were used to characterise the experimentally observed evolution of the stress pulse and compare it with the corresponding homogeneous reference specimens.

3. RESULTS AND DISCUSSION

3.1. Assessment of test validity

The validity of each impact test was assessed before any further time- or frequency-domain analysis. Particular attention was paid to the signals recorded by the two strain gauges positioned 180 ° apart at each measuring cross-section. Under approximately uniform axial loading, both gauges should record nearly identical

strain histories. A noticeable difference between the opposing signals indicates a non-uniform axial strain distribution, most likely caused by a small angular misalignment of the striker and imperfect parallelism of the contact surfaces.

The initial selection of valid impact tests was based on visual assessment of the agreement between the signals recorded by diametrically opposing strain gauges. To provide a quantitative verification of this selection, the normalised root mean square error (NRMSE) and Pearson correlation coefficient were subsequently evaluated for the paired signals at MP1. Since both strain gauges were of the same type and connected using identical measurement configurations, the analysis was performed directly on the recorded voltage signals. The NRMSE was calculated as

$$\mathrm{NRMSE} = \frac{\sqrt{\frac{1}{N}\sum_{i=1}^{N}\left(U_{1,i}-U_{2,i}\right)^2}}{\max\limits_{i}\left|\frac{U_{1,i}+U_{2,i}}{2}\right|} \times 100\,\%, \tag{3}$$

where $U_{1,i}$ and $U_{2,i}$ are the voltage signals recorded by the opposing strain gauges, and N is the number of samples in the analysed interval. The NRMSE characterises the overall difference between the signals, accounting for both amplitude and waveform discrepancies. The Pearson correlation coefficient was additionally used to characterise the similarity of the waveform shapes independently of their absolute amplitudes. Both parameters were evaluated over time windows that contained the first incident pulse, without changing the relative time of the opposing signals.

The originally accepted experiments exhibited NRMSE values ranging from 8.39 % to 20.01 %, with corresponding Pearson correlation coefficients ranging from 0.9023 to 0.9792. The rejected experiments showed substantially poorer agreement between the opposing signals, in some cases including opposite-phase responses. Based on this comparison, an empirical acceptance threshold of NRMSE $\leq 25\,\%$ was adopted to support the original visual assessment. The Pearson correlation coefficient was used as a supplementary indicator of waveform similarity, rather than as an independent acceptance criterion. The threshold was established retrospectively for the present experimental configuration and is not intended to be a universal criterion for Hopkinson-bar experiments.

This criterion was particularly important for MP1, which was located closest to the impacted end of the specimen. The use of the short 5 mm striker made the measurements sensitive to small deviations from a planar impact. Figure 5 compares representative strain-gauge records obtained for different impact conditions. In a valid test, the two opposing gauges at the same measuring position exhibit closely matching pulse shapes and amplitudes. In contrast, a clear separation of the two signals indicates an asymmetric loading state, and such measurements were excluded from the subsequent analysis.

High-speed camera imaging was used to provide an additional visual assessment of the impact event. However, the comparison shown in Figures 5 c) and e) demonstrates that small differences in impact alignment could not necessarily be visually identified from the acquired images. The strain-gauge pairs therefore provided a considerably more sensitive criterion for assessing impact quality. Only tests for which the paired signals showed satisfactory agree-

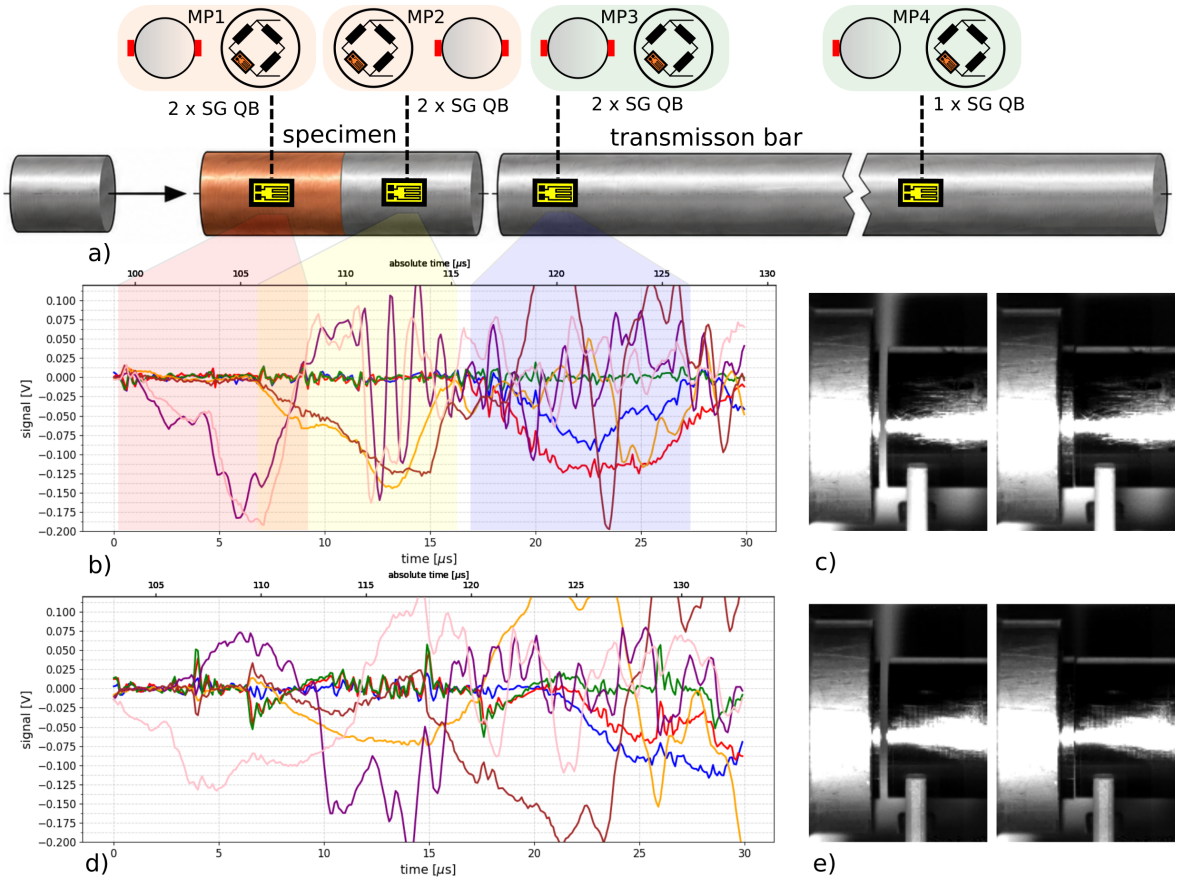


Figure 5. Assessment of impact-test validity based on the strain-gauge measurements: (a) arrangement of the measuring positions and paired strain gauges; (b) representative valid test showing close agreement between the signals from opposing gauges; (d) representative test affected by non-uniform loading, indicated by a pronounced difference between the opposing strain-gauge signals. High-speed images of the valid (c) and invalid (e) impacts did not reveal an equally clear difference between the two cases.

ment were retained for the subsequent averaging and comparison of the signals at MP1 and MP2.

3.2. Comparison with single-material reference specimens

The response of the multimaterial specimens was evaluated by comparison with the geometrically identical single-material reference specimens. During the experimental campaign, approximately 15 impacts per configuration were recorded after an initial visual assessment of the opposing strain-gauge signals. A considerably larger number of impacts were immediately rejected during testing because of pronounced discrepancies between these signals.

The recorded impacts were subsequently subjected to a more detailed evaluation of signal quality, supplemented by the retrospective NRMSE evaluation described in Section 3.1. Depending on the configuration, between three and seven valid repeated impacts were included in the final analysis. For each individual impact, the signals from the two strain gauges located at the same MP were first averaged. Before averaging the repeated experiments, the individual waveforms were aligned in time using a cross-correlation-based time shift. The resulting curves therefore represent the pointwise mean response obtained from repeated impacts on the same specimen, while the shaded regions indicate one standard deviation of these repeated measurements, rather than specimen-to-specimen variability. The same procedure was applied independently to MP1 and MP2. Compressive stress is shown with a negative sign.

The comparison was performed for both possible directions of wave propagation through the CuCr1Zr–13Ni400 interface. MP1 was located 15 mm before the interface, whereas MP2 was located 15 mm after the interface. Therefore, the response at MP1 contains the incident wave and possible contributions from waves reflected from the interface, whereas the response at MP2 represents the wave after interaction with the material interface and subsequent propagation through the second material.

Wave separation was considered but was not performed in the present study. Although two diametrically opposing strain gauges were used at each measuring position, they were located at the same axial coordinate, and therefore did not provide the spatially separated measurements required for conventional two-point wave separation. Consequently, the measured waveforms were analysed directly, without separating the incident and reflected wave components. The comparison with homogeneous reference specimens was therefore used to identify differences in the measured waveforms rather than to quantify the reflected wave independently. Model-assisted wave separation incorporating dispersive wave propagation and interface interactions will be investigated in future work. For the direction of propagation from CuCr1Zr to 13Ni400 (Figure 6), the MP1 response initially follows the homogeneous CuCr1Zr reference specimen. A deviation between the two responses develops during the later part of the compressive pulse, where the multimaterial specimens start to recover towards zero earlier than the reference. Since MP1 is located 15 mm before the interface, the reflected wave from the interface has to travel a total distance of 30 mm before reaching the MP again. Using the longitudinal wave velocity of CuCr1Zr of approximately 3386 m/s, calculated from the experimentally determined material properties, the expected return time of the reflected wave is approximately 8.9 μs. The observed deviation therefore occurs within the time range corresponding to the expected arrival of the reflected wave.

Based on the experimentally determined material properties, the one-dimensional impedance mismatch between CuCr1Zr and 13Ni400 predicts a positive stress reflection coefficient of

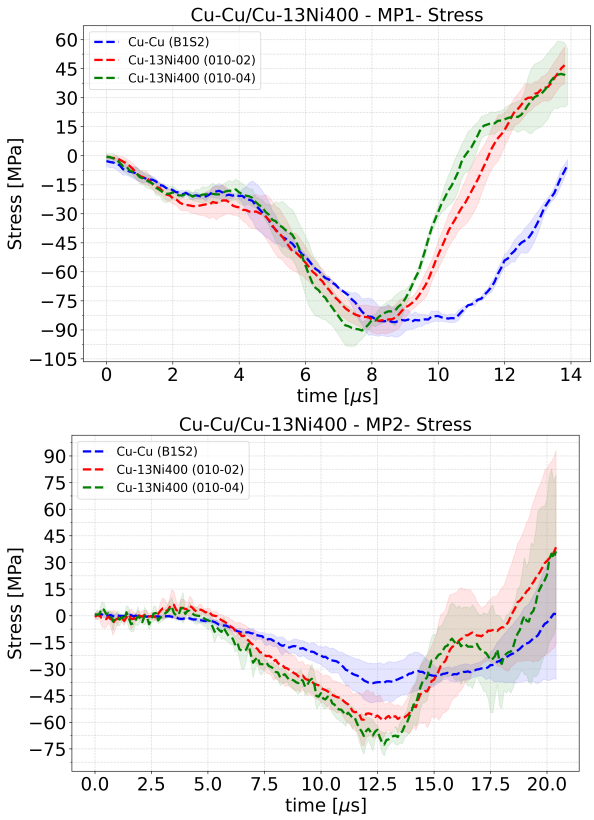


Figure 6. Stress histories for the CuCr1Zr–13Ni400 multimaterial configuration and CuCr1Zr single-material reference at MP1 (top) and MP2 (bottom).

approximately 22.1 %. This value provides only an estimate of the expected magnitude of the reflected component. The experimentally observed waveform cannot be explained solely by the one-dimensional impedance model, as the reflected component interacts with the short broadband pulse propagating through the cylindrical specimen. Therefore, the final waveform is affected by the temporal superposition of incident and reflected components together with the dispersive evolution of the pulse.

At MP2, the peak stress amplitude is reduced compared with MP1 for both the multimaterial and homogeneous reference specimens. However, despite the comparable initial responses at MP1, the multimaterial specimens exhibit higher peak compressive stresses at MP2 than the homogeneous CuCr1Zr reference. This behaviour is qualitatively consistent with the transmission of a stress wave from CuCr1Zr into the higher-impedance 13Ni400, for which the one-dimensional elastic model predicts an increase in the transmitted stress amplitude. Nevertheless, the measured differences cannot be attributed solely to the material interface, as the recorded waveforms are also influenced by dispersive propagation and wave superposition within the finite cylindrical specimens.

For the opposite propagation direction, from 13Ni400 to CuCr1Zr (Figure 7), the expected return time of the reflected wave at MP1 is approximately 6.1 μs, calculated using the longitudinal wave velocity of 13Ni400 of approximately 4916 m/s. The waveform changes between the multimaterial and homogeneous specimens occur within this time range; however, the effect of the reflected wave is less pronounced than for the opposite interface orientation.

For the 13Ni400–CuCr1Zr configuration, the peak stress amplitude is again reduced between MP1 and MP2. In contrast to the opposite propagation direction, the multimaterial specimen exhibits a lower maximum compressive stress at MP2 than the ho-

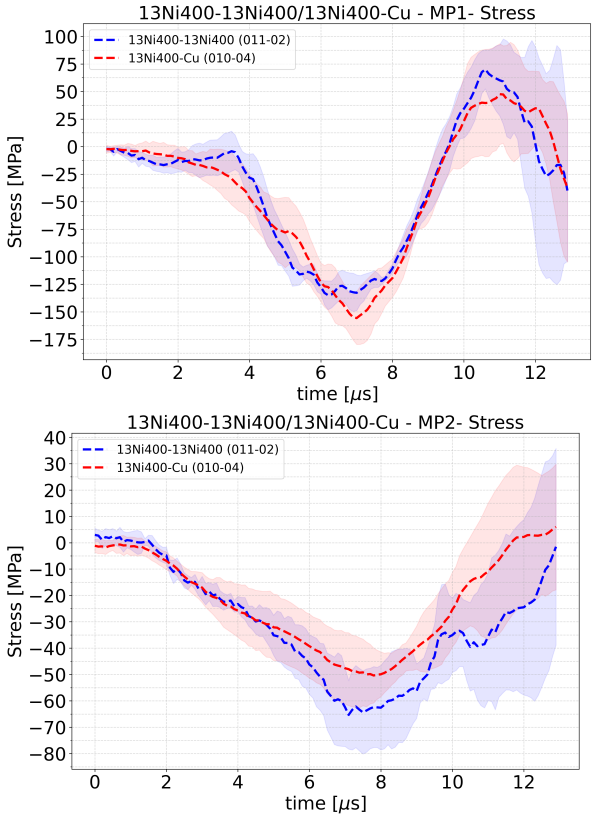


Figure 7. Stress histories for the 13Ni400–CuCr1Zr multimaterial configuration and 13Ni400 single-material reference at MP1 (top) and MP2 (bottom).

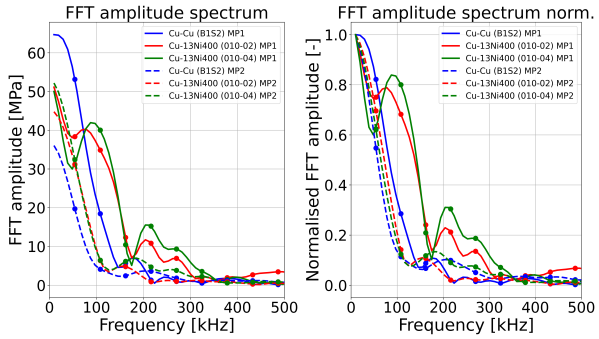


Figure 8. FFT amplitude spectra for the CuCr1Zr–13Ni400 configuration: absolute amplitudes (left) and normalised amplitudes (right) at MP1 and MP2.

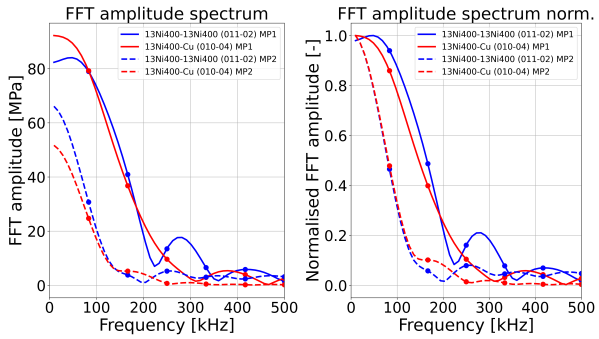


Figure 9. FFT amplitude spectra for the 13Ni400–CuCr1Zr configuration: absolute amplitudes (left) and normalised amplitudes (right) at MP1 and MP2.

mogeneous 13Ni400 reference. This observation is qualitatively consistent with wave transmission from a higher-impedance material into a lower-impedance material, for which the transmitted stress amplitude is expected to decrease. However, a reduction in stress amplitude between MP1 and MP2 is also observed in the homogeneous reference specimen, indicating that this reduction cannot be attributed solely to the material interface. The interface therefore introduces additional modifications of the waveform shape, amplitude, and timing superimposed on the effects of dispersive wave propagation within the finite specimen.

Overall, the comparison of both interface orientations shows that the material interface modifies the temporal evolution of the stress pulse. The time scale of the observed changes is consistent with the contribution of the reflected wave components; however, the resulting waveform is influenced by the broadband character of the generated pulse and by wave propagation in the cylindrical specimen.

To further examine these effects, the frequency content of the averaged stress histories at MP1 and MP2 was analysed using the FFT. The absolute and normalised amplitude spectra for the two interface orientations are presented in Figures 8 and 9, respectively. The absolute spectra show the change in spectral amplitude during propagation, whereas the normalised spectra allow the relative frequency content to be compared independently of the absolute stress amplitude.

For the CuCr1Zr–13Ni400 configuration (Figure 8), the MP1 spectra of the multimaterial specimens differ from the homogeneous CuCr1Zr reference. The normalised spectra show a higher relative spectral amplitude of the multimaterial specimens in the intermediate-frequency range of approximately 50–150 kHz. Since MP1 is located before the material interface, this difference is consistent with the modification of the measured pulse by the reflected wave. At MP2, the absolute spectral amplitude is substantially reduced for both the homogeneous and multimaterial specimens, while their normalised spectra become more similar.

Despite this overall reduction, the multimaterial specimens exhibit higher absolute spectral amplitudes at MP2 than the homogeneous CuCr1Zr reference over part of the investigated frequency range, consistent with the differences observed in the time-domain stress histories. The reduction in spectral amplitude between MP1 and MP2 observed in both homogeneous and multimaterial specimens indicates that this overall decrease is not specific to the presence of the material interface.

For the opposite direction of propagation, from 13Ni400 to CuCr1Zr (Figure 9), differences between the multimaterial specimen and the homogeneous reference are again observed at MP1. The normalised spectra show a modified distribution of the intermediate-frequency content, although the difference is less pronounced than for the CuCr1Zr–13Ni400 configuration. At MP2, the absolute spectra exhibit a substantial reduction in amplitude compared with MP1 for both the homogeneous and multimaterial specimens, while their normalised spectra become more similar. This reduction is therefore not specific to the presence of the material interface but also reflects the effects of wave propagation within the finite cylindrical specimen. Nevertheless, the multimaterial specimen exhibits lower absolute spectral amplitudes than the homogeneous 13Ni400 reference, particularly below approximately 100 kHz, consistent with the lower peak compressive stress observed in the time-domain response.

The similar evolution of the absolute spectra between MP1 and MP2 for homogeneous and multimaterial specimens indicates that propagation through the finite cylindrical specimen contributes substantially to the reduction of the measured high-frequency spectral amplitude. At the same time, the differences in the normalised MP1 spectra indicate modifications of the frequency content associated with the presence and orientation of the material interface. Furthermore, the absolute spectra at MP2

reveal orientation-dependent differences between the multimaterial specimens and their homogeneous references, consistent with the time-domain observations. The interface therefore does not act as a simple frequency filter but introduces additional spectral modifications superimposed on those caused by propagation and dispersion. The FFT results support the time-domain observations while demonstrating that the measured pulse evolution cannot be attributed to the material interface alone.

4. CONCLUSIONS

The experimental investigation of short stress-wave propagation across an LPBF-manufactured CuCr1Zr–13Ni400 material interface led to the following main conclusions:

- The use of two strain gauges positioned 180 ° apart provided a sensitive criterion for assessing impact validity and identifying non-uniform loading caused by imperfect alignment, even when no clear difference was visible in the corresponding high-speed camera recordings.
- The material interface modified the temporal evolution of the stress pulse. The observed deviations from the single-material reference occurred at times consistent with the expected arrival of reflected wave components.
- The measured response depended on the direction of wave propagation across the interface. At MP2, the CuCr1Zr–13Ni400 specimens exhibited higher peak compressive stresses than the homogeneous CuCr1Zr reference, whereas the opposite trend was observed for the 13Ni400–CuCr1Zr configuration. These observations are qualitatively consistent with the transmission of stress waves between materials with different mechanical impedances. A qualitative comparison of the measured waveforms at MP1 indicates more pronounced modifications of the pulse shape for the CuCr1Zr–13Ni400 configuration than for the reverse orientation.
- Similar reductions in stress and spectral amplitude between MP1 and MP2 were observed in both homogeneous and multimaterial specimens, demonstrating the significant influence of propagation and dispersion within the finite cylindrical specimen.
- FFT analysis revealed changes in the relative frequency content associated with the material interface, particularly at MP1 before the interface. Normalised spectra showed a higher relative contribution of intermediate frequencies for CuCr1Zr–13Ni400 multimaterial specimens. Furthermore, the absolute spectra at MP2 exhibited orientation-dependent differences between the multimaterial specimens and their corresponding homogeneous references, consistent with the time-domain observations.
- The observed response reflects the combined influence of the material interface, broadband excitation, dispersive propagation, and finite specimen geometry, highlighting the need to consider these effects when interpreting short stress-wave measurements.
- Numerical simulation represents a natural next step to distinguish the individual contributions of interface interaction, dispersive propagation, and finite specimen geometry. The authors have previous experience with numerical modelling of heterogeneous elastic-wave propagation and its application to Hopkinson-bar experiments [11], [12].

AUTHORS' CONTRIBUTION

Petr Zlámal: Conceptualisation, Methodology, Investigation, Analysis, Writing – original draft. **Jan Falta**: Investigation, Experimental setup validation, Writing – review & editing. **Radim Dvořák**: Investigation, Validation, Analysis, Writing – review & editing.

DATA AVAILABILITY STATEMENT

The raw experimental data supporting this study are publicly available in the Zenodo repository, DOI: 10.5281/zenodo.22825359.

ACKNOWLEDGMENT

The research was supported by the Czech Science Foundation in project no. 24-11505S.

REFERENCES

[1] A. Nazir, O. Gokcekaya, K. M. M. Billah, O. Ertugrul, J. Jiang, J. Sun, S. Hussain, Multi-material additive manufacturing: A systematic review of design, properties, applications, challenges, and 3D printing of materials and cellular metamaterials, Materials & Design, vol. 226, 2023, p. 111661. DOI: 10.1016/j.matdes.2023.111661

[2] O. Červinek, M. R. Tucker, D. Koutný, M. Bambach, Computational and experimental investigation of thermally auxetic multimetal lattice structures produced by laser powder bed fusion, Virtual and Physical Prototyping, vol. 19, 2024, no. 1, p. e2396069. DOI: 10.1080/17452759.2024.2396069

[3] Q. Sun, H.-b. Hu, Implementations and pilot comparison of primary low intensity shock calibration, Acta IMEKO, vol. 5, 2016, no. 3, pp. 70–75. DOI: 10.21014/acta_imeko.v5i3.314

[4] A. L. Shestakov, Dynamic measuring methods: a review, Acta IMEKO, vol. 8, 2019, no. 1, pp. 64–76. DOI: 10.21014/acta_imeko.v8i1.568

[5] R. Dvořák, J. Falta, P. Zlámal, P. Koudelka, J. Kopačka, J. Kylar, O. Jiroušek, Sample transfer function estimation of high-frequency elastic waves using Hopkinson bar, Measurement: Sensors, vol. 38, 2025, p. 101673. DOI: 10.1016/j.measen.2024.101673

[6] D. Bancroft, The velocity of longitudinal waves in cylindrical bars, Physical Review, vol. 59, 1941, no. 7, pp. 588–593. DOI: 10.1103/PhysRev.59.588

[7] A. Tyas, A. J. Watson, An investigation of frequency domain dispersion correction of pressure bar signals, International Journal of Impact Engineering, vol. 25, 2001, no. 1, pp. 87–101. DOI: 10.1016/S0734-743X(00)00025-7

[8] A. M. Bragov, A. K. Lomunov, D. A. Lamzin, A. Y. Konstantinov, Dispersion correction in split-Hopkinson pressure bar: theoretical and experimental analysis, Continuum Mechanics and Thermodynamics, vol. 34, 2022, pp. 895–907. DOI: 10.1007/s00161-019-00776-0

[9] A. D. Barr, S. E. Rigby, M. Clayton, Correction of higher mode Pochhammer–Chree dispersion in experimental blast loading measurements, International Journal of Impact Engineering, vol. 139, 2020, p. 103526. DOI: 10.1016/j.ijimpeng.2020.103526

[10] A. Fábry, M. Malý, M. Šmíd, M. Jambor, K. Dvořák, R. Kolman, D. Koutný, Interfacial characteristic of CuCr1Zr-Mar60 horizontal interface processed by LPBF, Abstract Book of the 1st MEBioSys Conference, Brno, Czech Republic, 2025, 9–10 September 2025. Online. [Accessed: 2026-11-14]. https://www.fme.vutbr.cz/etc/soubor/z/75712

[11] R. Dvořák, R. Kolman, T. Fíla, J. Falta, K. C. Park, Explicit asynchronous time scheme with local push-forward stepping for discontinuous elastic wave propagation: One-dimensional heterogeneous cases and Hopkinson bar experiment, Wave Motion, vol. 121, 2023, p. 103169. DOI: 10.1016/j.wavemoti.2023.103169

[12] R. Dvořák, L. Kocian, P. Koudelka, Performance analysis of an asynchronous time integration scheme for Split Hopkinson Pressure Bar simulations, Acta IMEKO, vol. 15, 2026, no. 3, pp. 1–8. DOI: 10.21014/actaimeko.v15i3.2459